Iranian Journal of Analytical Chemistry
Volume 12, Issue 2, September 2025 (12-28) Original Research Article

مجله ایرانی شیمی تجزیه
دوره ۱۲، شماره ۲، مهرماه ۱۴۰۴ (۲۸-۱۲)

β-Sitosterol from Allium cepa Seeds Exerts Dual-Target Anticancer Activity Against NFKB1 and STAT3 in Triple-Negative Breast Cancer: An Integrated In Silico and In Vitro Investigation

Sholeh Javadi [1], Somayeh Farahmand [1, *], Helia Bayat [1], Reza HajiHosseini [1], Sima Nasri [1]
Department of Biology, Payame Noor University, Tehran, Iran.

Received: 15 September 2025 Accepted**:** 21 September 2025
DOI: 10.30473/ijac.2026.77606.1345

Abstract
Triple-negative breast cancer (TNBC) lacks targetable receptors, rendering conventional chemotherapy the sole standard of care despite its associated toxicity and acquired resistance. The constitutively activated NF-κB and STAT3 signaling axes represent mechanistically interdependent oncogenic drivers in TNBC, making their simultaneous inhibition a compelling therapeutic strategy. β-Sitosterol, the predominant phytosterol of *Allium cepa* seeds, has demonstrated broad antiproliferative properties; however, its capacity for dual-target engagement against NFKB1 and STAT3 has not been systematically characterized. GC–MS profiling of *A. cepa* seed oil identified β-sitosterol as the principal constituent (80.45%). Computational ADMET analysis, Human Protein Atlas-based immunocytochemical target validation, and Auto Dock Vina molecular docking against NFKB1 (PDB: 5AX3) and STAT3 (PDB: 7LET) were performed. Anticancer activity was evaluated in MDA-MB-231 cells via MTT assay, with apoptotic mechanism characterized by Annexin V-FITC/PI flow cytometry. β-Sitosterol demonstrated favorable drug-likeness with predicted mitochondrial localization and absence of mutagenicity. Docking yielded binding energies of −7.0 and −6.7 kcal/mol for STAT3 and NFKB1, respectively, driven by hydrophobic interactions. MTT assay revealed concentration-dependent cytotoxicity (IC_{50} = 39.56 µM; 72 h; F = 113.8, $p < 0.0001$). Flow cytometry confirmed significant induction of early (30.7 ± 2.5%) and late apoptosis (20.3 ± 4.4%) versus negligible baseline levels in controls. β-Sitosterol exhibits dual computational binding affinity for NFKB1 and STAT3 alongside potent pro-apoptotic activity in TNBC cells, establishing a mechanistic foundation for its further translational development.

Keywords
β-sitosterol; Triple-negative breast cancer; NFKB1; STAT3; Apoptosis; MDA-MB-231.

1. INTRODUCTION

Breast cancer constitutes one of the most prevalent malignancies worldwide and remains the leading cause of cancer-related mortality among women globally, accounting for over 2.3 million new diagnoses and approximately 685,000 deaths annually according to the latest estimates from international health organizations [1]. Among its histological subtypes, triple-negative breast cancer (TNBC)—characterized by the absence of estrogen receptor (ER), progesterone receptor (PR), and human epidermal growth factor receptor 2 (HER2) expression—represents a particularly formidable clinical challenge [2, 3]. Constituting approximately 15–20% of all breast cancer cases, TNBC disproportionately afflicts younger women and those of African-American ancestry, and it is distinguished by its inherently aggressive biological behavior, high propensity for early visceral and central nervous system metastasis, and markedly inferior prognosis relative to receptor-positive subtypes [4]. The median overall survival of patients with advanced metastatic TNBC rarely exceeds 12 months under current treatment protocols, underscoring the urgent and unmet clinical need for novel, mechanism-based therapeutic interventions [5].

The absence of well-defined molecular targets renders TNBC uniquely refractory to the receptor-directed therapies that have transformed the management of other breast cancer subtypes, confining the standard-of-care approach to cytotoxic chemotherapy, which is burdened by significant off-target toxicity and the rapid development of acquired resistance [6]. Critically, the transcriptional landscape of TNBC is dominated by the constitutive activation of two oncogenic signaling axes—Nuclear Factor kappa B (NF-κB/NFKB1) and Signal Transducer and Activator of Transcription 3 (STAT3)—which

* Corresponding author:
Somayeh Farahmand; E-mail: fatemehsaber2003@pnu.ac.ir

operate in functional concert to sustain tumor cell survival, suppress apoptotic commitment, drive angiogenesis, promote epithelial-to-mesenchymal transition, and facilitate immune evasion [7]. The NF-κB pathway is frequently upregulated in TNBC, orchestrating the transcription of pro-survival and pro-inflammatory genes that collectively confer chemoresistance and support tumor cell persistence in hostile microenvironments [8]. STAT3, constitutively phosphorylated in a substantial proportion of TNBC tumors, amplifies this oncogenic program through the JAK/STAT axis, activating downstream effectors including Survivin, Mcl-1, and Bcl-2 that render tumor cells insensitive to apoptotic triggers [9]. The mechanistic crosstalk between these two pathways—wherein NF-κB-driven IL-6 secretion promotes JAK-dependent STAT3 phosphorylation, and activated STAT3 in turn reinforces NF-κB signaling through miR-21-mediated suppression of PDCD4—creates a self-sustaining oncogenic circuit that is extraordinarily difficult to dismantle through single-target approaches [10].

The persistent failure of conventional chemotherapeutic regimens to produce durable remission in TNBC, coupled with the mechanistic complexity of its oncogenic signaling networks, has accelerated interest in plant-derived bioactive compounds as alternative or complementary anticancer agents [11]. Natural phytochemicals offer the inherent advantage of engaging multiple cellular targets simultaneously through structurally diverse mechanisms, a property that positions them as particularly promising candidates for disrupting the kind of interlocked signaling circuits that characterize TNBC [12]. *Allium cepa L.* (common onion, family Alliaceae), one of the most globally cultivated and consumed vegetable species, harbors an extraordinarily diverse repertoire of bioactive secondary metabolites in its seeds, including organosulfur compounds, flavonoids, and phytosterols, that collectively endow it with well-documented antioxidant, anti-inflammatory, and anticarcinogenic properties [13]. Among its seed-derived lipid constituents, phytosterols—and β-sitosterol in particular—have emerged as phytochemicals of exceptional pharmacological relevance. β-Sitosterol (stigmast-5-en-3β-ol), a C-29 plant sterol sharing structural homology with cholesterol, has demonstrated broad-spectrum anticancer activity across multiple tumor models through mechanisms encompassing cell cycle arrest, caspase activation, mitochondrial membrane potential disruption, and modulation of key survival signaling pathways including the NF-κB and PI3K/Akt axes [14].

Despite the growing body of evidence supporting the anticancer potential of β-sitosterol, critical gaps persist in the literature regarding its specific mechanistic interactions with the NFKB1 and STAT3 oncogenic axes in TNBC, and its capacity for dual-target molecular engagement has not been systematically characterized through an integrated computational and experimental framework. Prior studies examining β-sitosterol in breast cancer cell models, while informative, have largely employed single-endpoint approaches or have not interrogated the precise molecular docking behavior of this phytosterol against structurally resolved breast cancer target proteins [15]. Furthermore, the phytosterol composition of *Allium cepa* seeds and the specific dominance of β-sitosterol within the seed lipid fraction have not been fully exploited as a rational basis for target-directed drug candidate selection. The pharmacokinetic and drug-likeness properties of β-sitosterol in the context of modern computational ADMET platforms also remain incompletely characterized in the specific context of TNBC-relevant protein targeting, leaving a substantial translational gap between phytochemical discovery and preclinical validation.

The present study addresses these research lacunae through a multi-tiered, evidence-based investigation that integrates GC–MS-guided phytochemical profiling of *Allium cepa* seed oil, computational ADMET pharmacokinetic evaluation, immunocytochemical characterization of NFKB1 and STAT3 expression from the Human Protein Atlas database, functional pathway analysis of the oncogenic signaling network, Auto Dock Vina-based molecular docking against crystallographically resolved target structures (PDB IDs: 7LET and 5AX3), and experimental validation through MTT cytotoxicity assay and Annexin V-FITC/PI flow cytometric apoptosis quantification in MDA-MB-231 TNBC cells. The primary innovation of this work lies in demonstrating, for the first time through an integrated in silico and in vitro pipeline, that β-sitosterol—the overwhelmingly dominant constituent (80.45%) of *Allium cepa* seed oil—possesses significant dual-binding affinity for NFKB1 and STAT3 simultaneously, and exerts potent concentration-dependent antiproliferative and pro-apoptotic effects against TNBC cells, thereby establishing a mechanistic and translational foundation for its further development as a dual-axis phytotherapeutic candidate in triple-negative breast cancer.

2. MATERIALS AND METHODS

2.1. Extraction and GC–MS Identification of β-Sitosterol from Allium cepa Seeds

Seeds of *Allium cepa L.* (family Alliaceae), characterized by their small, triangular, black, wrinkled morphology with a distinctive pungent

DOI: 10.30473/ijac.2026.77606.1345

odor and taste, were used as the botanical source for lipid extraction (herbarium voucher: NEU000100617). The seeds were thoroughly washed, shade-dried at ambient temperature for 72 hours, and subsequently pulverized to a fine homogeneous powder using an electric grinder. Lipid extraction was performed using ether (boiling point 40–60 °C) as the non-polar solvent, following standard cold maceration protocol. Approximately 10 seeds (total mass 35.7 g) were subjected to continuous extraction in a Soxhlet apparatus for 6 hours under reflux conditions, ensuring complete dissolution of all lipophilic constituents. Following extraction, the solvent was evaporated under reduced pressure at 40 °C using a rotary evaporator (Heidolph, Germany) to yield the crude oil extract. The resulting oil was transferred into amber glass vials and stored at −20 °C under nitrogen atmosphere until further analysis to prevent oxidative degradation of unsaturated fatty acid constituents [16].

The phytochemical composition of the extracted oil was characterized by gas chromatography–mass spectrometry (GC–MS) using a GC–MS system operating under optimized analytical conditions. The extracted oil was dissolved in n-hexane (HPLC grade) at a concentration of 1 mg/mL and filtered through a 0.22 µm PTFE membrane prior to injection. One microliter of the prepared sample was injected into the GC inlet in split mode (split ratio 1:10). Chromatographic separation was achieved on a non-polar capillary column (DB-5MS, 30 m × 0.25 mm × 0.25 µm) using helium as the carrier gas at a constant flow rate of 1.0 mL/min. The oven temperature program was set as follows: initial temperature 60 °C held for 2 minutes, ramped at 10 °C/min to 300 °C, and held isothermally for 10 minutes. The injector and ion source temperatures were maintained at 250 °C and 230 °C, respectively. Mass spectra were acquired in full scan mode over a mass range of m/z 50–600 with an electron ionization energy of 70 eV. Compound identification was performed by matching experimental mass spectra and retention indices against the NIST 2017 mass spectral library, with a minimum match threshold set at 90%. Relative abundance of each identified compound was calculated as the percentage of its peak area relative to the total ion chromatogram area [17, 18].

2.2. Target Selection and Functional Characterization

The subcellular localization and expression profiles of the two selected target proteins, NFKB1 and STAT3, were assessed using immunocytochemistry data retrieved from the Human Protein Atlas database (www.proteinatlas.org). For NFKB1, antibody HPA027305 (Atlas Antibodies / Sigma-Aldrich; rabbit polyclonal antibody; affinity-purified using PrEST-antigen as ligand; stock concentration 0.275 mg/ml) was applied to A-431, U-251MG, and U2OS cell lines fixed with paraformaldehyde (PFA) at dilutions of 1:100 (A-431 and U-251MG) and 1:137 (ciliated cell lines). For STAT3, antibody HPA001671 (Atlas Antibodies / Sigma-Aldrich; rabbit polyclonal antibody; affinity-purified using PrEST-antigen as ligand; stock concentration 0.03 mg/ml) was applied to the same cell panel (A-431, U-251MG, U2OS) at a uniform dilution of 1:15. Antibody specificity score was recorded as 5.0 for NFKB1 and 2.0 for STAT3. All staining procedures followed standardized immunofluorescence protocols with DAPI nuclear counterstaining and MitoTracker mitochondrial co-labeling to enable precise subcellular localization mapping. RNA expression values (nTPM) across cell lines were simultaneously documented to correlate protein abundance with transcriptional activity[19, 20].

To interrogate the oncogenic relevance of the selected targets, functional interaction and signaling network mapping were performed using curated pathway databases. The integrated signaling diagram was constructed to illustrate the crosstalk between the NF-κB and JAK/STAT3 axes, incorporating upstream regulatory elements including toll-like receptor (TLR) activation, miRNA-mediated regulatory nodes (miR-19, miR-21, miR-29b), and downstream transcriptional effectors. Key anti-apoptotic and pro-survival mediators including Survivin, Mcl-1, Bcl-2, and PDCD4 were mapped within the network to delineate the mechanistic basis for target selection. The functional schematic was constructed using pathway data from published literature and represented as a simplified regulatory diagram to highlight the dual-axis strategy underlying the study rationale.

2.3. Molecular Docking

Molecular docking was performed using Auto Dock Vina (version 1.1.2) [21] to evaluate the binding interactions between β-sitosterol and the two selected protein targets: STAT3 (PDB ID: 7LET) and NFKB1 (PDB ID: 5AX3). Protein three-dimensional structures were retrieved from the RCSB Protein Data Bank [22] and processed using AutoDockTools (ADT, version 1.5.7) [23]. Water molecules and co-crystallized ligands were removed from the crystal structures, hydrogen atoms were added, and Gasteiger partial charges were assigned. The docking grid coordinates were defined based on the native co-crystallized ligand-binding pockets of both crystal structures. To

DOI: 10.30473/ijac.2026.77606.1345

validate docking reliability, re-docking of the native ligands was performed prior to screening, and the resulting RMSD values were within acceptable thresholds (<2.0 Å), confirming the accuracy of the docking protocol. All rotatable bonds of β-sitosterol were defined as flexible, while the protein structures were treated as rigid. The three-dimensional structure of β-sitosterol was retrieved from the PubChem database (CID: 222284) and converted to PDBQT format using Open Babel (version 3.1.1) [24]. For the 7LET target, the docking search space was defined with a grid box centered at coordinates x = 1.5826, y = 23.6637, z = −0.5469, with box dimensions of 45.64 × 85.67 × 78.00 Å³. For the 5AX3 target, the grid box was centered at x = 8.1222, y = −13.1403, z = −20.1643, with dimensions of 59.46 × 53.39 × 67.53 Å³, encompassing the entire active site cavity. The exhaustiveness parameter was set to 8 for both targets to ensure adequate conformational sampling. Docking was run with 9 output poses per run, and the pose yielding the lowest binding free energy was selected for further analysis. Visualization of the three-dimensional binding pose and generation of two-dimensional ligand–protein interaction diagrams were performed using LigPlot+ (version 2.2.4) [25], enabling identification of hydrophobic contacts and hydrogen bond interactions between the ligand and surrounding residues[25-27].

2.4. Drug-Likeness and ADMET Analysis

The pharmacokinetic and drug-likeness properties of β-sitosterol were computationally evaluated using the ADMETsar 3.0 online prediction server (http://lmmd.ecust.edu.cn/admetsar3) [28, 29]. The canonical SMILES string of β-sitosterol was submitted as input. The following parameters were systematically assessed: subcellular localization prediction, molecular weight, blood–brain barrier (BBB) permeability, human oral bioavailability, nephrotoxicity, hepatotoxicity, and Ames mutagenicity. Each parameter was expressed as a probability score accompanied by a binary classification outcome. Radar chart visualization of physicochemical descriptors—including molecular weight (MW), number of atoms (nAtom), number of rings (nRing), number of rotatable bonds (nRot), number of hydrogen bond acceptors (nHBA), hydrogen bond donors (HBD), topological polar surface area (TPSA), and lipophilicity (SlogP)—was generated within the ADMETsar 3.0 interface and compared against standard drug-like upper and lower boundary domains to assess overall compound suitability for pharmaceutical development [30-32].

2.5. MTT Assay

Metabolic viability was quantified using the MTT colorimetric reduction assay. MDA-MB-231 triple-negative breast cancer cells were seeded into flat-bottom 96-well tissue culture plates at a density of 5×10^3 cells per well in 100 µL complete DMEM medium supplemented with 10% fetal bovine serum and 1% penicillin/streptomycin, and allowed to adhere overnight at 37 °C in a humidified 5% CO_2 incubator. Following the adherence period, the culture medium was replaced with fresh medium containing serial concentrations of β-sitosterol (6.25, 12.5, 25, 50, and 100 µM), prepared by serial dilution from a stock solution dissolved in dimethyl sulfoxide (DMSO). Control wells received only the vehicle solvent (DMSO, maximum final concentration 0.1% v/v). After 72 hours of incubation, MTT reagent (3-(4,5-dimethylthiazol-2-yl)-2,5-diphenyltetrazolium bromide) was added to each well to a final concentration of 0.5 mg/mL, and plates were returned to the incubator for an additional 4 hours to permit intracellular formazan crystal formation by metabolically active cells. Culture medium was carefully aspirated, and the insoluble purple formazan precipitate was dissolved in 100 µL DMSO with gentle agitation for 15 minutes. Absorbance was measured spectrophotometrically at 570 nm using an ELX808IU microplate reader (Biotek, USA). Percentage cell viability was calculated by normalizing treated well absorbance values to those of the untreated control wells, which were defined as 100% viability. The half-maximal inhibitory concentration (IC_{50}) was determined by nonlinear regression analysis of dose-response curves using GraphPad Prism version 5.0 [33].

2.6. Flow Cytometric Analysis of Apoptosis

Apoptotic cell death was quantified using dual fluorescent staining with Annexin V-FITC and propidium iodide (PI) according to the manufacturer's protocol (BioLegend, USA). Following 72-hour treatment with β-sitosterol at its IC_{50} concentration, both adherent and floating cells were harvested. Culture supernatants containing detached cells were collected, and adherent cells were detached by trypsinization. The combined cell suspensions were washed twice with ice-cold phosphate-buffered saline (PBS) and resuspended in 1× Annexin V Binding Buffer at a concentration of approximately 1×10^6 cells/mL. A 100 µL aliquot of each cell suspension was transferred to flow cytometry tubes and co-incubated with 5 µL Annexin V-FITC and 10 µL PI solution in the dark at room temperature for 15 minutes. Subsequently, 400 µL of 1× Binding Buffer was added to each tube, and samples were immediately analyzed using a BD FACSCalibur flow cytometer (Becton Dickinson, USA) equipped with a 488 nm argon laser excitation source. A minimum of 10,000 events were

DOI: 10.30473/ijac.2026.77606.1345

acquired per sample. Data acquisition and subsequent analysis were performed using FlowJo software (TreeStar Inc., USA). Cell populations were classified into four distinct quadrants: viable cells (Annexin V^-/PI^-), early apoptotic cells (Annexin V^+/PI^-), late apoptotic cells (Annexin V^+/PI^+), and necrotic cells (Annexin V^-/PI^+). Statistical analysis was performed using GraphPad Prism version 5.0, with one-way ANOVA followed by Tukey's post-hoc test applied for multiple group comparisons [34].

3. RESULTS

3.1 Phytochemical Composition and Identification of the Major Bioactive Constituent

GC–MS analysis of the ether extract obtained from *Allium cepa L.* seeds (Fig. 1A) revealed a chromatographic profile dominated by a limited number of steroidal compounds, as illustrated in the total ion chromatogram presented in Fig. 1B. Quantitative analysis of the nine identified constituents, summarized in Table 1, demonstrated a striking compositional hierarchy wherein β-sitosterol emerged as the overwhelmingly predominant component, accounting for 80.45% of the total chromatographic area, with a characteristic retention time of 28.8 minutes and a peak area of 3,040,420,482 arbitrary units. The second most abundant sterol was campesterol (RT: 23.86 min; 10.18%), followed by cycloartanol (RT: 29.18 min; 6.94%), which together constituted the core steroidal matrix of the extract. Minor constituents included 2,4-methylenecycloartanol (0.93%), gamma-sitosterol (0.56%), cycloeucalenol (0.27%), cholest-7-enol (0.22%), stigmasterol (0.29%), and cholesterol (0.16%), each present at quantities below 1% of the total composition. The marked dominance of β-sitosterol relative to all other detected compounds unequivocally identifies it as the principal bioactive phytochemical constituent of *Allium cepa* seed oil and provides a robust phytochemical rationale for its selection as the candidate ligand for subsequent computational and biological investigations. The two-dimensional chemical structure of β-sitosterol, featuring the characteristic C-29 ethyl sterol backbone with a hydroxyl group at C-3 position of the cyclopentanoperhydrophenanthrene ring system, is presented in Fig. 1C, consistent with its well-documented capacity to engage hydrophobic binding domains within target proteins.

Table 1. GC–MS analysis of the ether extract obtained from *Allium cepa L.* seeds

No	Component	Peak	Area	RT%
1	Compestrol	384792122	23.86	10.18
2	B-sitosterol	3040420482	28.8	80.45
3	Cycloartanol	262405643	29.18	6.94
4	Cholest-7-enol	8246862	29.4	0.22
5	Cycloeucalenol	10175149	33.75	0.27
6	2,4-methylencycloartanol	35059522	34.6	0.93
7	Cholesterol	6156215	40.44	0.16
8	Stigmaterol	10843310	40.9	0.29
9	Gamma-Sitosterol	21135341	61.08	0.56

3 2. Drug-Likeness and ADMET Profile of β-Sitosterol

Computational pharmacokinetic profiling of β-sitosterol performed through the ADMETsar 3.0 platform yielded a comprehensive set of predictions presented in Table 2, with graphical representation of physicochemical and compound property parameters illustrated in Fig. 1D and Fig. 1E respectively. Subcellular localization analysis predicted preferential mitochondrial distribution; an observation of notable mechanistic relevance given the central role of mitochondria in orchestrating intrinsic apoptotic signaling cascades. The molecular weight of β-sitosterol was determined as 414.71 Da, placing it within an acceptable range for membrane-permeable bioactive compounds, although marginally exceeding the classical Lipinski threshold—a characteristic that is well-tolerated in phytosterol pharmacology due to compensatory structural features. Regarding systemic distribution, the compound was predicted to be blood–brain barrier permeable (positive prediction), indicating adequate lipophilicity for CNS penetration, though this parameter is of secondary relevance in the context of breast cancer targeting. Human oral bioavailability was predicted with a probability score of 0.6714, classified as positive under the high-bioavailability threshold, which reflects the good intestinal absorption characteristic of phytosterols and is consistent with published clinical pharmacokinetic data for this compound class. From a safety perspective, the toxicity predictions were particularly favorable: β-sitosterol demonstrated a negative Ames mutagenicity, confirming the complete absence of predicted genotoxic activity, and exhibited a negative nephrotoxicity and hepatotoxicity prediction, indicating no anticipated renal and Liver adverse effects. The radar chart in Fig. 1D-E illustrates the positioning of β-sitosterol's physicochemical descriptors relative to the drug-

DOI: 10.30473/ijac.2026.77606.1345

like upper and lower boundary domains, confirming that the compound's overall molecular property profile falls within or proximal to acceptable pharmaceutical space. Collectively, the ADMET analysis supports the classification of β-sitosterol as a pharmacologically viable candidate warranting further experimental evaluation, and provides a sound basis for proceeding with cellular and molecular investigations.

Table 2. The result of AdmetSAR database.

Name of the drug	Admet SAR						
	Subcellular localization	Molecular Weight	Blood Brain Barrier	Human Oral Bioavailability	Nephrotoxicity	Hepatotoxicity	Ames Mutagenesis
β -sitosterol	Mitochondria	414.71	+	0.6714 **(+)**	0.7820 **(-)**	0.8725 **(-)**	0.9300 **(-)**

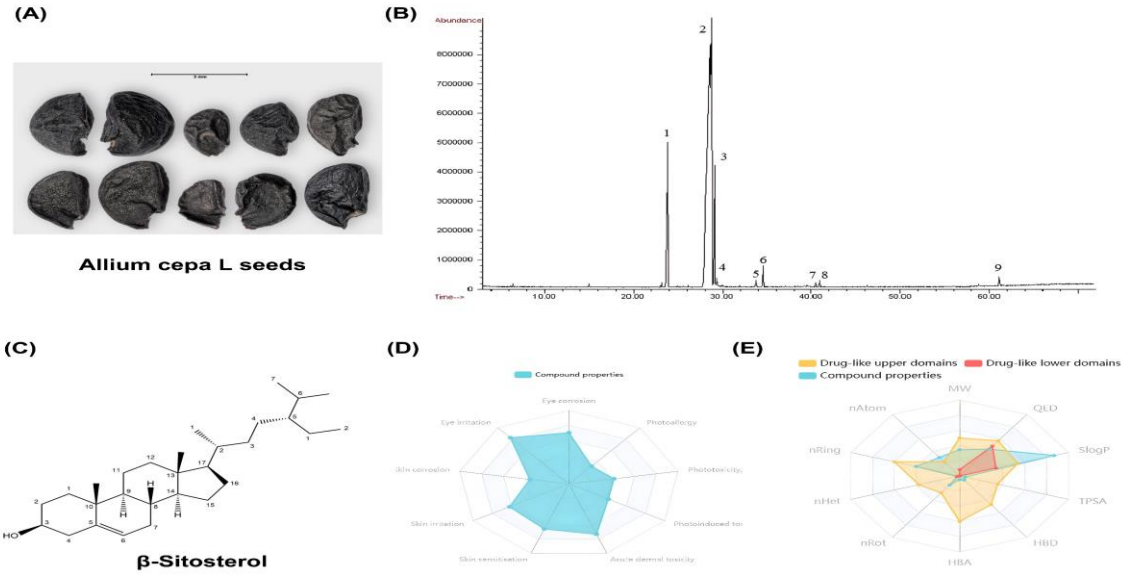

Fig. 1. (A) *Allium cepa L*. seeds. (B) GC–MS total ion chromatogram of seed oil extract. (C) 2D chemical structure of β-sitosterol. (D–E) Radar charts of physicochemical and ADMET properties generated by ADMETsar 3.0.

3.3. Expression Profiling and Oncogenic Significance of NFKB1 and STAT3

Immunocytochemical analysis performed using validated antibodies from the Human Protein Atlas database revealed robust and consistent expression of both NFKB1 and STAT3 across the panel of human cell lines examined, as depicted in Fig. 2A. For NFKB1, staining with antibody HPA027305 demonstrated prominent fluorescence signal in the nucleoplasm and cytosol of A-431 cells (RNA expression: 35.6 nTPM), U-251MG cells (14.1 nTPM), and U2OS cells (12.1 nTPM), with an additional mitochondrial localization component detected specifically in U2OS cells. The nucleoplasmic distribution of NFKB1 is indicative of its transcriptionally active state and underscores its function as a nuclear transcription factor that, upon activation, translocates from the cytoplasm to the nucleus to drive expression of pro-survival and pro-inflammatory gene programs. For STAT3, staining with antibody HPA001671 revealed an exclusively nucleoplasmic and cytosolic distribution pattern across all three cell lines, with notably higher RNA expression values: 65.2 nTPM in A-431, 74.7 nTPM in U-251MG, and 45.6 nTPM in U2OS cells. The substantially elevated STAT3 transcript levels compared to NFKB1 across all tested cell lines indicate a high baseline transcriptional activity of STAT3, reinforcing its established role as a constitutively active oncogenic driver in multiple cancer contexts. The consistent dual-compartment localization of both proteins across divergent cell line models confirms their broad oncogenic relevance and validates their selection as therapeutic targets.

The functional significance of these two proteins within the breast cancer signaling landscape is comprehensively illustrated in the pathway schematic presented in Fig. 2B. The diagram delineates an interconnected regulatory network in which NF-κB and STAT3 operate as convergent

DOI: 10.30473/ijac.2026.77606.1345

transcriptional hubs that together coordinate oncogenic output across multiple dimensions. Upstream activation proceeds through toll-like receptor (TLR) engagement by inflammatory stimuli such as LPS, which promotes NF-κB activation through PDCD4 signaling and concurrently induces IL-6 secretion. IL-6, acting through the canonical JAK/STAT3 axis, drives STAT3 phosphorylation and nuclear translocation, while suppressor of cytokine signaling 1 (SOCS1) provides a negative feedback checkpoint that is itself subject to regulation by miR-19 and miR-29b. Activated STAT3 promotes transcription of key anti-apoptotic effectors including Survivin, Mcl-1, and Bcl-2, which collectively suppress the apoptotic machinery and sustain tumor cell viability. Concurrently, both NF-κB and STAT3 converge on miR-21 upregulation, which further amplifies oncogenic signaling by suppressing tumor suppressor targets such as PTEN, Rho-B, and BTG2, thereby reinforcing an anti-apoptotic, pro-proliferative transcriptional program. The downstream consequences include enhanced cell growth, proliferation, and survival, while apoptotic commitment is actively suppressed. Critically, PDCD4 downregulation—driven by miR-21 activity—creates a feedback loop that sustains both NF-κB and STAT3 activation through TNF-α and IL-10 mediated signals, effectively locking tumor cells into a state of constitutive survival signaling. The functional architecture illustrated in Fig. 2B thus reveals that NF-κB and STAT3 are not merely parallel targets but rather mutually reinforcing components of a unified oncogenic network. A therapeutic agent capable of interfering with both axes simultaneously would be expected to produce a substantially more comprehensive disruption of cancer cell survival than single-target approaches, providing a compelling mechanistic rationale for the dual-target strategy adopted in the present study.

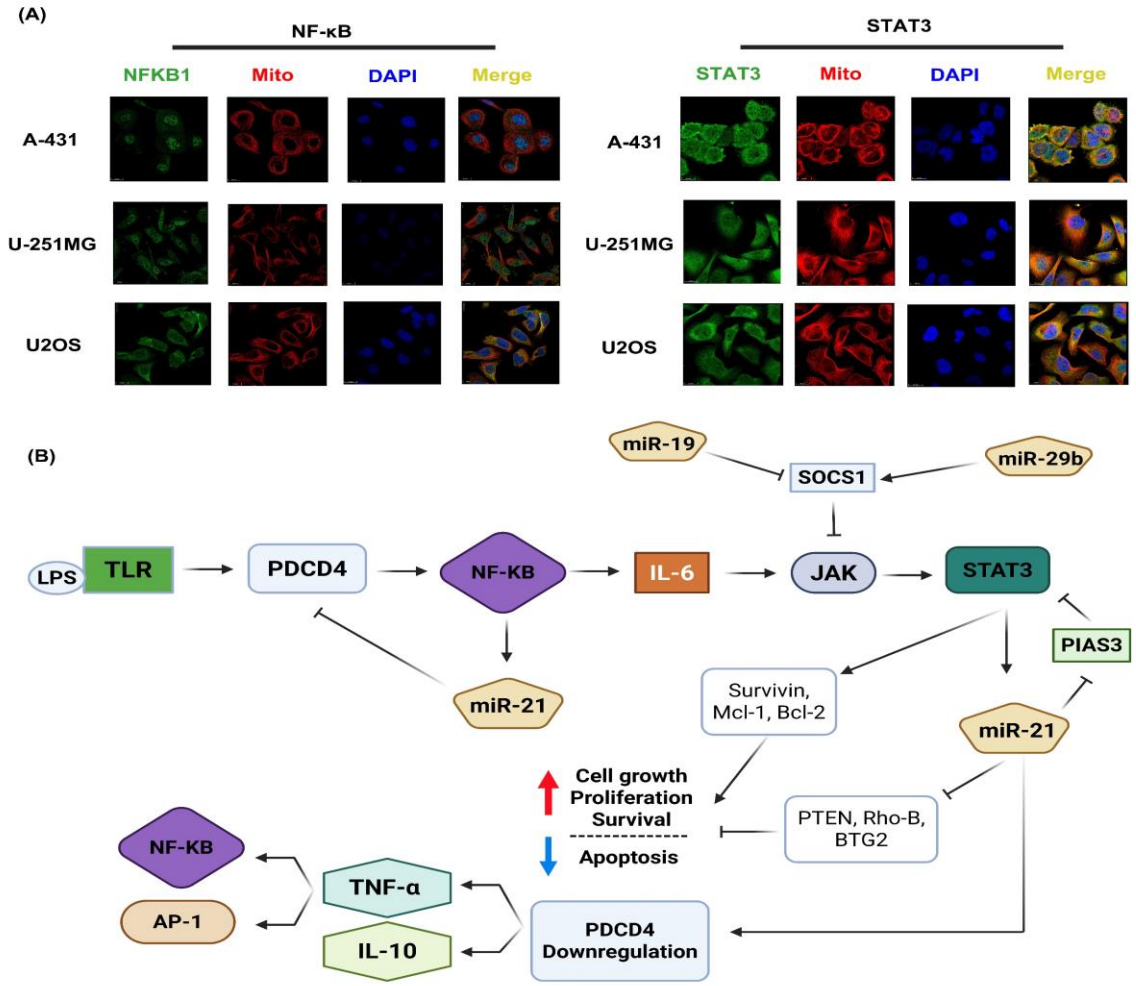

Fig. 2. (A) Immunocytochemical localization of NFKB1 and STAT3 in A-431, U-251MG, and U2OS cell lines (B) Functional signaling network illustrating NF-κB/STAT3 oncogenic crosstalk in breast cancer.

DOI: 10.30473/ijac.2026.77606.1345

3.4. Molecular Docking and Binding Interaction Analysis

Molecular docking analysis performed using AutoDock Vina revealed that β-sitosterol establishes energetically favorable interactions with both selected protein targets, as illustrated in Fig. 3. For the STAT3-related structure represented by PDB ID 7LET (Fig. 3A), β-sitosterol docked with a calculated binding free energy of −7.0 kcal/mol. The three-dimensional binding pose illustrates that the ligand occupies a well-defined hydrophobic pocket within the protein interior, with its steroidal scaffold positioned in close proximity to the helical secondary structure elements of the binding site. The two-dimensional interaction map generated by LigPlot+ revealed that complex stabilization was predominantly mediated by hydrophobic interactions and van der Waals contacts. Because β-sitosterol contains only a single hydroxyl functional group and forms predominantly non-polar interactions within both binding pockets, precise bond-distance reporting was not considered mechanistically critical to the interpretation of the docking results.

For the NFKB1 structure represented by PDB ID 5AX3 (Fig. 3B), β-sitosterol produced a binding energy of −6.7 kcal/mol. The surface electrostatic map illustrates docking within a predominantly electropositive binding region, and the three-dimensional pose confirms stable accommodation of the sterol within a cleft bordered by alpha-helical elements. The corresponding LigPlot+ two-dimensional interaction diagram demonstrates a broader network of hydrophobic contacts compared to 7LET, with additional van der Waals interactions distributed across a larger set of contacting residues, consistent with the larger grid box dimensions employed for this target. The slightly higher binding affinity observed for 7LET (−7.0 kcal/mol) relative to 5AX3 (−6.7 kcal/mol) suggests a marginally more favorable geometric and energetic complementarity between β-sitosterol and the STAT3-associated binding site, though both values fall within the range considered indicative of significant ligand–protein affinity. The demonstrated capacity of β-sitosterol to engage both targets with comparable binding energies provides strong in silico evidence for its dual-target inhibitory potential and supports the hypothesis that this phytosterol may simultaneously perturb both the NF-κB and STAT3 signaling axes in cancer cells.

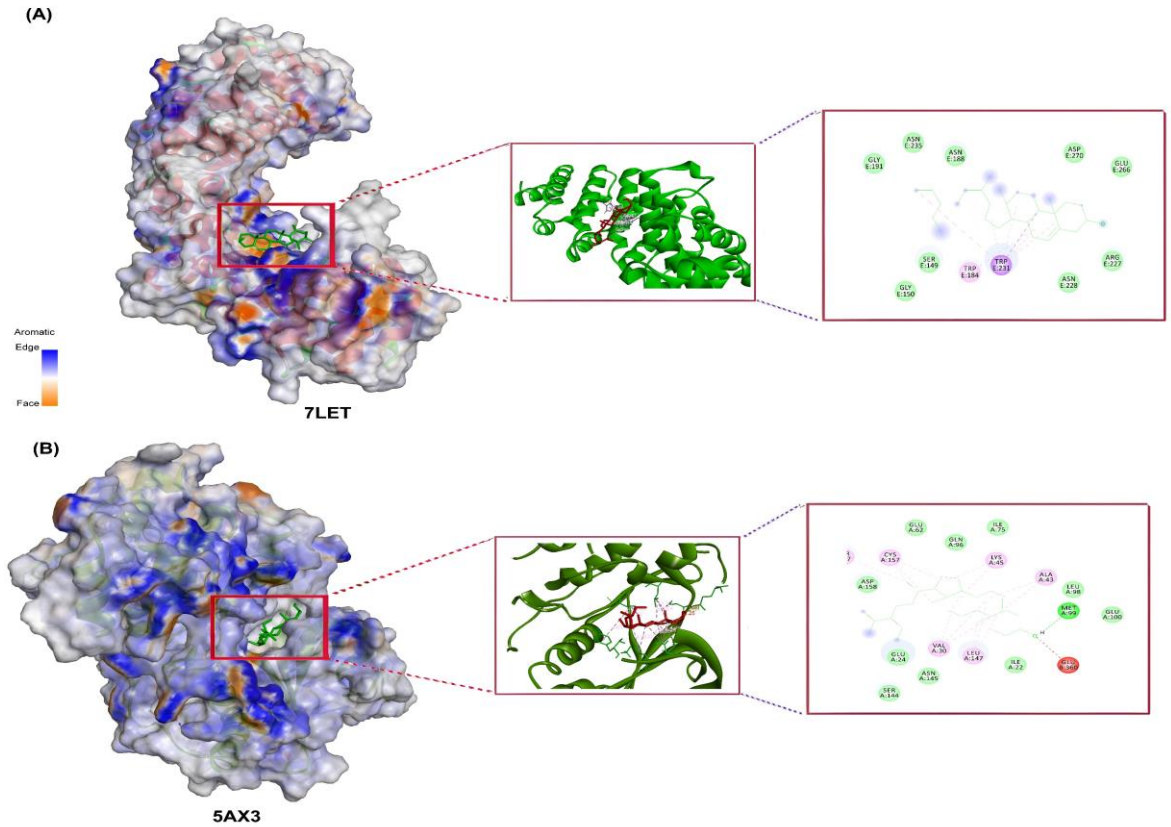

Fig. 3. Molecular docking of β-sitosterol with (A) STAT3 (PDB: 7LET; −7.0 kcal/mol) and (B) NFKB1 (PDB: 5AX3; −6.7 kcal/mol). Left: surface electrostatic map; center: three-dimensional binding pose; right: LigPlot+ two-dimensional interaction diagram.

DOI: 10.30473/ijac.2026.77606.1345

3.5. Cytotoxic Activity of β-Sitosterol in MDA-MB-231 Cells

MTT assay results presented in Fig. 4A demonstrate that β-sitosterol exerts a pronounced concentration-dependent reduction in the metabolic viability of MDA-MB-231 triple-negative breast cancer cells following 72-hour exposure. At the lowest tested concentration of 6.25 µM, cell viability remained relatively high at approximately 85%, indicating minimal cytotoxic impact at sub-therapeutic concentrations. Progressive increases in concentration produced a consistent and statistically significant decline in viability, with values of approximately 75%, 65%, 50%, and 25% recorded at 12.5, 25, 50, and 100 µM respectively. Nonlinear regression analysis of the dose–response relationship yielded an IC_{50} value of 39.56 µM, identifying this concentration as the pivotal threshold at which β-sitosterol suppresses the proliferative capacity of MDA-MB-231 cells by 50% relative to untreated controls. One-way ANOVA confirmed highly significant intergroup differences across the concentration series ($F = 113.8$, $p < 0.0001$), validating the statistical robustness of the observed dose–response relationship. The smooth, monotonic nature of the inhibition curve across the tested concentration range is indicative of a single-mode mechanism of growth suppression, and the IC_{50} value obtained falls within a pharmacologically achievable range, lending translational credibility to these findings. These results establish the concentration-dependent antiproliferative capacity of β-sitosterol against triple-negative breast cancer cells and provide the quantitative basis for concentration selection in subsequent mechanistic investigations.

3.6. Induction of Apoptosis by β-Sitosterol

Flow cytometric analysis using dual Annexin V-FITC/PI staining provided mechanistic insight into the mode of cell death induced by β-sitosterol at its IC_{50} concentration following 72-hour treatment. In untreated control cultures (Fig. 4C), the vast majority of cells occupied the viable quadrant (Annexin V^-/PI^-), with background levels of early apoptosis (Annexin V^+/PI^-) and late apoptosis (Annexin V^+/PI^+) recorded at 3.6 ± 2.6% and 0.8 ± 0.6%, respectively, confirming the baseline integrity of the cell population under standard culture conditions. Treatment with β-sitosterol at its IC_{50} concentration (Fig. 4B) induced a dramatic and statistically significant redistribution of the cell population away from the viable fraction toward apoptotic compartments. The early apoptotic population increased markedly to 30.7 ± 2.5%, representing an approximately 8.5-fold elevation relative to control values ($p < 0.0001$). The late apoptotic fraction concurrently rose to 20.3 ± 4.4%, reflecting a greater than 25-fold increase over baseline ($p < 0.0001$). The quadrant distribution pattern observed in Fig. 4B is thus characterized by a prominent accumulation of cells in the Annexin V^+ compartments, providing unequivocal evidence for the activation of phosphatidylserine externalization—a hallmark biochemical event of early apoptotic commitment—as the primary mode of cell death.

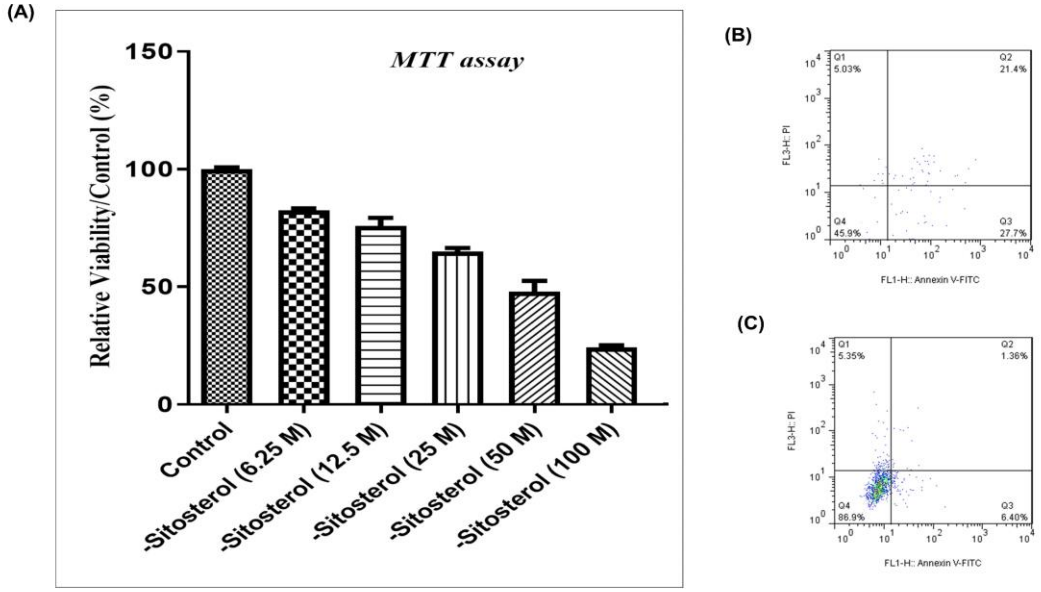

Fig. 4. (A) MTT assay: dose-dependent cell viability of MDA-MB-231 cells following 72-hour β-sitosterol treatment. (B–C) Flow cytometric Annexin V-FITC/PI analysis of (B) β-sitosterol-treated and (C) untreated control MDA-MB-231 cells.

DOI: 10.30473/ijac.2026.77606.1345

The predominant shift toward early apoptosis, with early apoptotic cells outnumbering late apoptotic cells in the β-sitosterol-treated population, suggests that the compound initiates apoptotic signaling with high efficiency at early commitment checkpoints, consistent with its predicted mitochondrial localization from ADMET analysis and its putative inhibitory interactions with STAT3 and NF-κB survival pathways demonstrated in the docking studies. The negligible necrotic fraction observed in treated cells confirms that the observed reduction in cell viability is attributable to regulated apoptotic cell death rather than non-specific membrane disruption or cytolytic toxicity, reinforcing the mechanistic specificity of β-sitosterol's anticancer action.

4. Discussion

The present study developed and validated an integrated computational–experimental strategy for evaluating β-sitosterol, the principal phytosterol constituent of *Allium cepa L.* seed oil, as a candidate dual-target anticancer agent against NFKB1 and STAT3 in triple-negative breast cancer. The cumulative findings across phytochemical, computational, and cellular experimental domains converge to construct a coherent mechanistic narrative that warrants detailed interpretation.

The GC–MS profiling of the ether extract obtained from *A. cepa* seeds yielded a sterol-rich composition in which β-sitosterol was detected as the overwhelmingly predominant constituent, accounting for 80.45% of total chromatographic area at a retention time of 28.8 minutes. The remaining fraction comprised structurally related sterols including campesterol (10.18%) and cycloartanol (6.94%), with minor contributions from stigmasterol, gamma-sitosterol, cholesterol, and cycloeucalenol, each below 1%. This compositional profile is consistent with the known phytosterol signature of *Allium* species, in which β-sitosterol, campesterol, cycloartenol, and stigmasterol constitute the dominant sterol matrix of seed lipids [35]. The remarkable degree of β-sitosterol dominance observed in the present extract—exceeding 80%—is especially noteworthy and provides an exceptionally clean phytochemical rationale for its selection as the candidate ligand, as the pharmacological activity of the crude extract can be attributed with high confidence to this single major constituent. The structural features of β-sitosterol, particularly its tetracyclic steroid backbone with an ethyl substituent at C-24 and a hydroxyl group at C-3, confer strong amphiphilicity and the capacity to engage hydrophobic binding domains within protein active sites—a property that forms the biophysical foundation for its computational interaction with the target proteins evaluated in the present study [36].

The ADMET computational profiling of β-sitosterol revealed a pharmacokinetic profile that, when considered holistically, supports its further biological investigation. The prediction of preferential subcellular localization within the mitochondrial compartment is of particular mechanistic interest, given the central role of mitochondria in coordinating the intrinsic apoptotic cascade through cytochrome c release, Apaf-1 apoptosome assembly, and downstream caspase activation [37]. This predicted mitochondrial tropism is consistent with published evidence demonstrating that β-sitosterol treatment induces depolarization of the mitochondrial membrane potential in MDA-MB-231 cells, an event associated with altered Bax/Bcl-2 ratios and commitment to intrinsic apoptosis [38]. The positive prediction for blood–brain barrier permeability reflects the high lipophilicity of the compound, while the negative Ames mutagenicity prediction provides strong in silico evidence for the absence of genotoxic liability, a critical safety attribute for any drug candidate advancing toward translational development. The negative nephrotoxicity and hepatotoxicity prediction further support the acceptable safety profile, this finding is not atypical for lipophilic phytosterols and does not preclude further development, particularly given the established clinical safety record of dietary β-sitosterol consumption in human populations [39]. Taken together, the ADMET data position β-sitosterol within a pharmacologically viable space, justifying its progression to target-specific experimental investigation.

The immunocytochemical characterization of NFKB1 and STAT3 using Human Protein Atlas antibodies confirmed robust expression of both targets across the panel of tested cell lines. NFKB1 displayed a nucleoplasmic and cytosolic distribution in A-431 cells at 35.6 nTPM, U-251MG at 14.1 nTPM, and U2OS at 12.1 nTPM, with an additional mitochondrial localization component in U2OS. STAT3 exhibited exclusively nucleoplasmic and cytosolic distribution with significantly higher transcript levels, reaching 74.7 nTPM in U-251MG and 65.2 nTPM in A-431. The substantially elevated STAT3 expression relative to NFKB1 across all tested lines aligns with the well-documented finding that STAT3 is constitutively overexpressed and phosphorylated in TNBC, where it functions as a master transcriptional regulator of tumor cell survival, proliferation, immune evasion, and stemness maintenance [40, 41]. The nucleoplasmic localization of both proteins confirms their transcriptionally active states and underscores their functional relevance as

DOI: 10.30473/ijac.2026.77606.1345

drivers of the oncogenic gene expression programs that sustain tumor cell survival. The functional pathway schematic in Fig. 2B reveals that NFKB1 and STAT3 are not functionally independent entities but rather mutually reinforcing arms of a convergent oncogenic circuit. NF-κB activation drives IL-6 secretion, which in turn stimulates JAK-mediated STAT3 phosphorylation; activated STAT3 then promotes miR-21 expression, which suppresses PDCD4 and tumor suppressors PTEN and Rho-B, further amplifying NF-κB transcriptional activity through a positive feedback mechanism [42]. This bidirectional crosstalk implies that inhibiting either target in isolation would be subject to compensatory upregulation through the remaining pathway—a mechanistic argument that strongly justifies a dual-target inhibitory strategy and contextualizes the rationale for selecting a phytosterol with demonstrated affinity for both binding sites.

The molecular docking results provide compelling in silico evidence for the capacity of β-sitosterol to engage both target proteins with energetically significant affinity. Against the STAT3-associated structure (PDB: 7LET), a binding free energy of −7.0 kcal/mol was calculated, while the NFKB1 structure (PDB: 5AX3) yielded −6.7 kcal/mol. Both values are situated within the range generally accepted as indicative of meaningful ligand–protein interaction in structure-based drug discovery [43]. The marginally higher affinity for 7LET is consistent with the structural features of the STAT3 binding domain, which presents a well-defined hydrophobic SH2-adjacent pocket that accommodates the non-polar steroidal scaffold of β-sitosterol with favorable van der Waals complementarity. The LigPlot+ two-dimensional interaction maps confirm that binding in both cases is predominantly mediated by hydrophobic contacts and van der Waals forces rather than polar hydrogen bonding, which is expected given the lipophilic nature of the sterol backbone. These interaction profiles are mechanistically congruent with previously reported in silico findings demonstrating that β-sitosterol forms stable hydrophobic complexes with key oncogenic proteins, including those involved in NF-κB and PI3K/Akt signaling cascades [44]. The simultaneous affinity of a single phytomolecule for both NFKB1 and STAT3 at binding energies below −6.5 kcal/mol is particularly noteworthy, as it suggests a structurally enabled dual-inhibitory mechanism that could produce additive or potentially synergistic pathway suppression in a cellular context.

The in vitro cytotoxicity results obtained by MTT assay confirm the antiproliferative efficacy of β-sitosterol in MDA-MB-231 TNBC cells in a robust, dose-dependent manner. The IC_{50} value of 39.56 μM after 72-hour exposure represents a pharmacologically meaningful threshold of activity. This value is comparable to IC_{50} values reported for β-sitosterol-mediated growth inhibition in MDA-MB-231 cells in prior investigations, including the range of 30–90 μM employed by Vundru et al. to demonstrate G1 cell cycle arrest accompanied by CDK4 and cyclin D1 downregulation and p21/Cip1 upregulation [45]. The progressive, monotonic inhibition curve across the 6.25–100 μM concentration range, confirmed by one-way ANOVA ($F = 113.8$, $p < 0.0001$), is characteristic of a compound acting through a unified mechanism of proliferative suppression rather than through concentration-dependent cytolytic toxicity. This type of smooth dose-response relationship is mechanistically more consistent with the modulation of survival signaling pathways—such as NFKB1 and STAT3—than with non-specific membrane disruption, aligning with the molecular docking predictions presented in the present study. The IC_{50} value obtained also falls within a range that is considered pharmacologically relevant for phytosterol-based candidates, particularly in the context of in vitro systems where cellular uptake and bioavailability are not rate-limiting [46]. Previous studies have primarily reported the anticancer activity of β-sitosterol through mechanisms such as cell-cycle arrest, mitochondrial dysfunction, and apoptosis induction in breast cancer models. However, most prior investigations did not integrate phytochemical profiling, dual-target molecular docking against both NFKB1 and STAT3, ADMET evaluation, and apoptosis validation within a unified experimental framework. Therefore, the present study extends existing evidence by proposing a dual-pathway mechanistic model for β-sitosterol in triple-negative breast cancer.

Flow cytometric analysis using Annexin V-FITC/PI dual staining provided decisive mechanistic evidence that the cytotoxic activity of β-sitosterol is mediated through the activation of apoptotic cell death programs rather than non-specific cytolytic toxicity. Treatment at the IC_{50} concentration for 72 hours produced a marked shift in population distribution, with early apoptotic cells (Annexin V^+/PI^-) increasing from a basal level of 3.6 ± 2.6% in untreated controls to 30.7 ± 2.5% in treated cells—an approximately 8.5-fold amplification ($p < 0.0001$)—and late apoptotic cells rising from 0.8 ± 0.6% to 20.3 ± 4.4% ($p < 0.0001$). The predominant accumulation of cells within the early apoptotic quadrant indicates that β-sitosterol initiates phosphatidylserine externalization—the defining biochemical hallmark of early apoptotic commitment—at high

DOI: 10.30473/ijac.2026.77606.1345

efficiency, while a significant proportion of cells subsequently proceed to the late apoptotic stage. This apoptotic kinetics pattern is consistent with activation of the intrinsic mitochondrial pathway, congruent with the predicted mitochondrial localization of β-sitosterol from ADMET analysis and with prior evidence demonstrating that β-sitosterol induces mitochondrial membrane potential depolarization and elevated Bax/Bcl-2 ratios in breast cancer cells [47]. The negligible necrotic population in treated samples confirms the mechanistic selectivity of the compound's cytotoxic action. This apoptotic profile is mechanistically explicable through the putative inhibitory interactions of β-sitosterol with NFKB1 and STAT3 identified in the docking analysis: suppression of NFKB1 transcriptional activity would be expected to reduce expression of anti-apoptotic Bcl-family members and IAP proteins, while concurrent STAT3 inhibition would diminish Survivin and Mcl-1 expression, collectively lowering the apoptotic threshold and sensitizing tumor cells to programmed death commitment—precisely the pattern observed in the flow cytometric data of the present study [48].

Considered in its entirety, this investigation establishes a coherent mechanistic framework in which β-sitosterol, extracted at dominant abundance from *Allium cepa* seeds and validated through GC–MS compositional analysis, engages two pivotal oncogenic transcription factors—NFKB1 and STAT3—through energetically favorable molecular interactions, demonstrates a drug-like pharmacokinetic profile, and exerts significant concentration-dependent antiproliferative and pro-apoptotic effects in triple-negative breast cancer cells. The dual-target binding capacity demonstrated in silico, combined with the in vitro evidence of apoptosis induction through what appears to be a mitochondria-mediated mechanism, positions β-sitosterol as a highly promising phytosterol candidate for further development within the framework of TNBC targeted therapy. Future investigations should focus on validating the molecular targets of β-sitosterol through protein expression analysis, including Western blotting of NFKB1 and STAT3 phosphorylation states following treatment, as well as extending the mechanistic characterization to include caspase activation profiling, cell cycle distribution analysis, and assessment of mitochondrial membrane potential. In vivo xenograft studies and structure-activity relationship investigations of β-sitosterol derivatives with enhanced bioavailability will be essential to translate the present findings toward a clinically actionable therapeutic candidate. A limitation of the present study is the absence of comparative cytotoxicity evaluation in non-malignant breast epithelial cells, which prevents definitive conclusions regarding the cancer-selective safety profile of β-sitosterol. Future studies should investigate its therapeutic selectivity using normal breast cell models.

5. CONCLUSIONS

The present investigation provides a comprehensive, multi-layered body of evidence demonstrating that β-sitosterol, isolated as the overwhelmingly dominant phytosterol constituent of *Allium cepa* seed oil through GC–MS-guided phytochemical profiling, possesses concurrent in silico binding affinity for both NFKB1 and STAT3 oncogenic targets at pharmacologically significant binding free energies, exhibits a favorable ADMET pharmacokinetic profile characterized by predicted mitochondrial tropism and absence of genotoxic liability, and exerts potent concentration-dependent antiproliferative and pro-apoptotic effects in MDA-MB-231 triple-negative breast cancer cells, as evidenced by an IC_{50} of 39.56 µM and a marked shift toward early and late apoptotic cell populations confirmed by Annexin V-FITC/PI flow cytometry, collectively establishing this phytosterol as a mechanistically rationalized dual-axis therapeutic candidate whose further validation through in vivo xenograft models, Western blot-based target engagement studies, and structure-activity relationship analyses represents a scientifically well-grounded and clinically meaningful priority in the pursuit of novel targeted interventions against this therapeutically refractory malignancy.

Declaration of interest

There are no conflicts to declare. The authors report no conflicts of interest. Also, the authors are responsible for the writing and content of this article.

Acknowledgments

This research is derived from a doctoral dissertation. The authors sincerely thank all esteemed professors, particularly Dr. Saber SamadiAfshar, for their valuable guidance, constructive feedback, and continuous support throughout all stages of this research—from initial conceptualization to data analysis.

REFERENCES

[1] F. Bray. M. Laversanne. H. Sung. J. Ferlay. R.L. Siegel. I. Soerjomataram and A. Jemal. Global cancer statistics 2022: GLOBOCAN estimates of incidence and mortality worldwide for 36 cancers in 185 countries. CA Cancer J. Clin. 74(3) (2024) 229-263. https://doi.org/10.3322/caac.21834

[2] S. Kim. D.H. Kim. W. Lee. Y.M. Lee. S.Y. Choi and K. Han. The nature of triple-negative breast cancer classification and antitumoral

strategies. Genomics Inform. 18(4) (2020) e35. https://doi.org/10.5808/gi.2020.18.4.e35

[3] S. Farahmand. S. SamadiAfshar. M. Khalili and R. Haji Hosseini. Therapeutic implications of Epirubicin-induced miRNA-22 and miRNA-331 upregulation on cell viability and metastatic potential in triple-negative breast cancer. Hum. Gene. 44 (2025) 201396. https://doi.org/https://doi.org/10.1016/j.humgen.2025.201396

[4] N. Jinna. Y.C. Yuan and P. Rida. Kinesin Family Member C1 (KIFC1/HSET) Underlies Aggressive Disease in Androgen Receptor-Low and Basal-Like Triple-Negative Breast Cancers. Int. J. Mol. Sci. 24(22) (2023). https://doi.org/10.3390/ijms242216072

[5] V. Peirce. M. Paskow. L. Qin. R. Dadzie. M. Rapoport. S. Prince and S. Johal. A Systematised Literature Review of Real-World Treatment Patterns and Outcomes in Unresectable Advanced or Metastatic Biliary Tract Cancer. Target Oncol. 18(6) (2023) 837-852. https://doi.org/10.1007/s11523-023-01000-5

[6] N. Dasari. G.S. Guntuku and S. Pindiprolu. Targeting triple negative breast cancer stem cells using nanocarriers. Discov. Nano. 19(1) (2024) 41. https://doi.org/10.1186/s11671-024-03985-y

[7] J.H. Kim. S. Park. E. Jung. J. Shin. Y.J. Kim. J.Y. Kim JL. Sessler. JH. Seo. and JS. Kim. A dual-action niclosamide-based prodrug that targets cancer stem cells and inhibits TNBC metastasis. Proc. Natl. Acad. Sci. U.S.A. 120(21) (2023) e2304081120. https://doi.org/10.1073/pnas.2304081120

[8] V. De Paolis. V. Troisi. A. Bordin. F. Pagano. V. Caputo and C. Parisi. Unconventional p65/p52 NF-κB module regulates key tumor microenvironment-related genes in breast tumor-associated macrophages (TAMs). Life Sci. 357 (2024) 123059. https://doi.org/10.1016/j.lfs.2024.123059

[9] M.Y. Kuo. W.T. Yang. Y.J. Ho. G.M. Chang. H.H. Chang. C.Y. Hsu. C.C.Chang. and Y.H. Chen. Hispolon Methyl Ether, a Hispolon Analog, Suppresses the SRC/STAT3/Survivin Signaling Axis to Induce Cytotoxicity in Human Urinary Bladder Transitional Carcinoma Cell Lines. Int. J. Mol. Sci. 24(1) (2022). https://doi.org/10.3390/ijms24010138

[10] Z. Li. Q. Xia. Y. He. L. Li and P. Yin. MDSCs in bone metastasis: mechanisms and therapeutic potential. Cancer Lett. (2024) 216906. https://doi.org/10.1016/j.canlet.2024.216906

[11] L.I. Gavrilas. D. Cruceriu. A. Mocan. F. Loghin. D. Miere and O. Balacescu. Plant-Derived Bioactive Compounds in Colorectal Cancer: Insights from Combined Regimens with Conventional Chemotherapy to Overcome Drug-Resistance. Biomedicines. 10(8) (2022). https://doi.org/10.3390/biomedicines10081948

[12] K. Pandit. C. Garg. A.H. Bhat. R. Bhardwaj and S. Kaur. Harnessing Dietary Phytochemicals to Modulate Signaling Pathways in Cancer Chemoprevention-A Review. Phytother. Res. 39(7) (2025) 3271-3299. https://doi.org/10.1002/ptr.8524

[13] J.K. Yan. J. Zhu. Y. Liu. X. Chen. W. Wang. H. Zhang and L.Li. Recent advances in research on Allium plants: functional ingredients, physiological activities, and applications in agricultural and food sciences. Crit. Rev. Food Sci. Nutr. 63(26) (2023) 8107-8135. https://doi.org/10.1080/10408398.2022.2056132

[14] O.A. Rozentsvet. E.R. Kotlova. E.S. Bogdanova. V.N. Nesterov. S.V. Senik and A.L. Shavarda. Balance of Δ(5)-and Δ(7)-sterols and stanols in halophytes in connection with salinity tolerance. Phytochemistry. 198 (2022) 113156. https://doi.org/10.1016/j.phytochem.2022.113156

[15] A.J. Siddiqui. S. Elkahoui. A.M. Alshammari. M. Patel. A.E.M. Ghoniem. R.A.H. Abdalla. H. Dwivedi-Agnihotri. R. Badraoui. and M.Adnan. Mechanistic Insights into the Anticancer Potential of Asparagus racemosus Willd. Against Triple-Negative Breast Cancer: A Network Pharmacology and Experimental Validation Study. Pharmaceuticals (Basel). 18(3) (2025). https://doi.org/10.3390/ph18030433

[16] D.C. de Faria. M. de Queiroz and F.J.M. Novaes. Direct Hot Solid-Liquid Extraction (DH-SLE): A High-Yield Greener Technique for Lipid Recovery from Coffee Beans. Plants (Basel). 14(2) (2025). https://doi.org/10.3390/plants14020185

[17] S. Samadiafshar. S. Farahmand. A. Nikakhtar. N. Garmsiri. F. Garmsiri. S. Samadiafshar and R.Azizi. Antibacterial and Phytochemical Properties of Stachys schtschegleevii Oil Extract: Investigating Interaction and Antimicrobial Activity against Urinary Tract Infection Bacteria Through in Silico and in Vitro. Iran. J. Anal. Chem. 12(1) (2025). https://doi.org/10.30473/ijac.2025.75318.1324

[18] X. Wang. J. Li. S. Jiang. W. Shen. Y. Wang and Q. Gu. Simultaneous determination of monochloropropanediol esters and glycidyl esters in vegetable oils by acidic transesterification-gas chromatography-mass spectrometry. Se Pu. 40(2) (2022) 198-205. https://doi.org/10.3724/sp.j.1123.2021.05009

[19] M. Masoudi. S. Samadiafshar. H. Azizi and T. Skutella. Integrated Analysis, Machine Learning, Molecular Docking and Dynamics of CDK1 Inhibitors in Epithelial Ovarian Cancer: A Multifaceted Approach Towards Targeted Therapy. Int. J. Mol. Sci. 26(18) (2025). https://doi.org/10.3390/ijms26189168

[20] H. Jin. C. Zhang. M. Zwahlen. K. von Feilitzen. M. Karlsson. M. Shi. M. Yuan. X. Song. X. Li. H. Yang and H. Turkez. Systematic transcriptional analysis of human cell lines for gene expression landscape and tumor representation. Nat. Commun. 14(1) (2023) 5417. https://doi.org/10.1038/s41467-023-41132-w

[21] Eberhardt. J. Santos-Martins. D. Tillack. AF. Forli. S. AutoDock Vina 1.2.0: New Docking Methods, Expanded Force Field, and Python Bindings. J Chem Inf Model. 2021 Aug 23;61(8):3891-3898. https://doi.org/10.1021/acs.jcim.1c00203

[22] Berman. H. Henrick. K. Nakamura. H. Markley. JL. The worldwide Protein Data Bank (wwPDB): ensuring a single, uniform archive of PDB data. Nucleic Acids Res. 2007 Jan;35(Database issue): D301-3. https://doi.org/10.1093/nar/gkl971

[23] El-Hachem. N. Haibe-Kains. B. Khalil. A. Kobeissy. FH. Nemer. G. AutoDock and AutoDockTools for Protein-Ligand Docking: Beta-Site Amyloid Precursor Protein Cleaving Enzyme 1(BACE1) as a Case Study. Methods Mol Biol. 2017; 1598:391-403. https://doi.org/10.1007/978-1-4939-6952-4_20

[24] O'Boyle. NM. Banck. M. James. CA. Morley. C. Vandermeersch. T. Hutchison. GR. Open Babel: An open chemical toolbox. J Cheminform. 2011 Oct 7; 3:33. https://doi.org/10.1186/1758-2946-3-33

[25] S. Farahmand. S. SamadiAfshar. R. HajiHosseini and T. Babari. Carnosic Acid as a Potent Ag85C Inhibitor Identified Through Integrated Pharmacokinetic Evaluation and Molecular Modeling in Mycobacterium Tuberculosis Drug Discovery. J. Pharm. Innov. 20(6) (2025) 275. https://doi.org/10.1007/s12247-025-10191-5

[26] R.A. Laskowski and M.B. Swindells. LigPlot+: multiple ligand-protein interaction diagrams for drug discovery. J. Chem. Inf. Model. 51(10) (2011) 2778-2786. https://doi.org/10.1021/ci200227u

[27] S. Farahmand. S. SamadiAfshar and L. Hosseini. TA-Cloning for Diabetes Treatment: Expressing Corynebacterium Malic Enzyme Gene in E. coli. Curr. Microbiol. 81(6) (2024) 167. https://doi.org/10.1007/s00284-024-03686-w

[28] S. SamadiAfshar. A. NikAkhtar. S. SamadiAfshar and S. Farahmand. Antibacterial Property of Silver Nanoparticles Green Synthesized from Stachys schtschegleevii Plant Extract on Urinary Tract Infection Bacteria. Curr. Microbiol. 81(5) (2024) 135. https://doi.org/10.1007/s00284-024-03664-2

[29] H. Yang. C. Lou. L. Sun. J. Li. Y. Cai. Z. Wang. W. Li. G. Liu. and Y.Tang. admetSAR 2.0: web-service for prediction and optimization of chemical ADMET properties. Bioinformatics. 35(6) (2019) 1067-1069. https://doi.org/10.1093/bioinformatics/bty707

[30] S. Farahmand. S. SamadiAfshar and N.A. Shahmoradi. Electrospun PCL/PVP Nanofibers Meshes, A Novel Bisabolol Delivery System for Antidermatophytic Treatment. J. Pharm. Innov. 20(1) (2025) 25. https://doi.org/10.1007/s12247-025-09928-z

[31] I. Sungur. N. Bayar Muluk. C. Vejselova Sezer. H.M. Kutlu and C. Cingi. Efficacy and toxicity of anise oil as a potential topical wound healer: a cell culture study. Eur. Rev. Med. Pharmacol. Sci. 27(2 Suppl) (2023) 14-20. https://doi.org/10.26355/eurrev_202303_31696

[32] Gu. Y. Yu. Z. Wang. Y. Chen. L. Lou. C. Yang. C. Li. W. Liu. G. Tang. Y. admetSAR3.0: a comprehensive platform for exploration, prediction and optimization of chemical ADMET properties. Nucleic Acids Res. 2024 Jul 5;52(W1): W432-W438. https://doi.org/10.1093/nar/gkae298

[33] SamadiAfshar. S. Azizi. H. Masoudi. M. SamadiAfshar. S. Nikakhtar. A. Skutella. T. Preoperative differentiation of borderline and malignant ovarian tumors using interpretable machine learning. J Ovarian Res. 2026 Apr 15. https://doi.org/10.1186/s13048-026-02062-5

[34] R. Mouna. A. Broisat. M. Debiossat. A. Boumendjel. C. Ghezzi and Z. Kabouche. Evaluation of antiproliferative activity, apoptotic induction and LC-HRMS/MS analyses of the VLC fractions of L. numidicum. Nat. Prod. Res. 37(5) (2023) 788-792. https://doi.org/10.1080/14786419.2022.2084738

[35] K. Kulik and B. Waszkiewicz-Robak. Comparison of Changes in Sterol Content of Nuts After Roasting Using Conventional and Microwave Methods and After Storage. Molecules. 30(3) (2025). https://doi.org/10.3390/molecules30030606

[36] N. Deshwal. M.B. Singh. I. Bahadur. N. Kaushik. N.K. Kaushik. P. Singh and K. Kumari. A review on recent advancements on removal of harmful metal/metal ions using graphene oxide: Experimental and theoretical approaches. Sci. Total Environ. 858(Pt 1)

(2023) 159672. https://doi.org/10.1016/j.scitotenv.2022.159672

[37] L. Galluzzi. I. Vitale. S.A. Aaronson. J.M. Abrams. D. Adam. P. Agostinis. ES. Alnemri. L. Altucci. I. Amelio. DW. Andrews. and M. Annicchiarico-Petruzzelli. Molecular mechanisms of cell death: recommendations of the Nomenclature Committee on Cell Death 2018. Cell Death Differ. 25(3) (2018) 486-541. https://doi.org/10.1038/s41418-017-0012-4

[38] J. Rajendran. P. Pachaiappan and R. Thangarasu. Citronellol, an Acyclic Monoterpene Induces Mitochondrial-Mediated Apoptosis through Activation of Proapoptotic Factors in MCF-7 and MDA-MB-231 Human Mammary Tumor Cells. Nutr. Cancer. 73(8) (2021) 1448-1458. https://doi.org/10.1080/01635581.2020.1800766

[39] B.H. Yoon. V.L. Truong and W.S. Jeong. Phytosterols: Extraction Methods, Analytical Techniques, and Biological Activity. Molecules. 30(12) (2025). https://doi.org/10.3390/molecules30122488

[40] J. Li. R. Gao and J. Zhang. USP22 Contributes to Chemoresistance, Stemness, and EMT Phenotype of Triple-Negative Breast Cancer Cells by regulating the Warburg Effect via c-Myc Deubiquitination. Clin. Breast Cancer. 23(2) (2023) 162-175. https://doi.org/10.1016/j.clbc.2022.11.006

[41] J. Mou. X. Xu. F. Wang. W. Kong. J. Chen and J. Ren. HMGN4 plays a key role in STAT3-mediated oncogenesis of triple-negative breast cancer. Carcinogenesis. 43(9) (2022) 874-884. https://doi.org/10.1093/carcin/bgac056

[42] L. Wu. Y. Chai. A. Gao. Y. Lin. J. Han. L. Li. C. Li. and J. Ye. IL-21 signaling promotes IgM(+) B cell proliferation and antibody production via JAK/STAT3 and AKT pathways in early vertebrates. Dev. Comp. Immunol. 164 (2025) 105325. https://doi.org/10.1016/j.dci.2025.105325

[43] A.F.A. Hidayat and S.B. Mohamad. Incorporating Target Protein Structure Flexibility and Dynamics in Computational Drug Discovery Using Ensemble-Based Docking Analysis. J. Vis. Exp. 220 (2025). https://doi.org/10.3791/67174

[44] T. Jiang. S. Bo. Y. You. Y. Wang. L. Hou. S. Tian. B. Bai. Y. Cheng. and Y. Gao. ELAVL1 facilitates gastric cancer progression and metastasis through TL1A mRNA stabilization. Exp. Cell Res. 446(2) (2025) 114491. https://doi.org/10.1016/j.yexcr.2025.114491

[45] S.S. Vundru. R.K. Kale and R.P. Singh. β-Sitosterol induces G1 arrest and causes depolarization of mitochondrial membrane potential in breast carcinoma MDA-MB-231 cells. BMC Complement. Altern. Med. 13 (2013) 280. https://doi.org/10.1186/1472-6882-13-280

[46] S. Cho. Y. Jung. S.J. Rho and Y.R. Kim. Stability, bioavailability, and cellular antioxidant activity of piperine complexed with cyclic glucans. Food Sci. Biotechnol. 34(11) (2025) 2475-2488. https://doi.org/10.1007/s10068-025-01884-1

[47] J. Kim. K. Kim. D. Park. S.K. Eo. B.A. Lee and Y. Son. 25-Hydroxycholesterol Induces Intrinsic Apoptosis via Mitochondrial Pathway in BE(2)-C Human Neuroblastoma Cells. Int. J. Mol. Sci. 26(16) (2025). https://doi.org/10.3390/ijms26168012

[48] S. Jayaraman. S.R. Natarajan. B. Ponnusamy. V.P. Veeraraghavan and S. Jasmine. Unlocking the potential of beta sitosterol: Augmenting the suppression of oral cancer cells through extrinsic and intrinsic signalling mechanisms. Saudi Dent. J. 35(8) (2023) 1007-1013. https://doi.org/10.1016/j.sdentj.2023.08.003

بتا-سیتوسترول استخراج‌شده از دانه‌های پیاز (Allium cepa) از طریق مهار همزمان NFKB1 و STAT3 با اثر ضد سرطانی دو محوره در سرطان پستان سه‌گانه منفی(TNBC): بررسی یکپارچه سلیکو و آزمایشگاهی

شعله جوادی[1]، سمیه فرهمند[1,*]، هلیا بیات[1]، رضا حاجی حسینی[1]، سیما نصری[1]

گروه زیست شناسی، دانشگاه پیام نور، تهران، ایران

* E-mail: s.farahmand@pnu.ac.ir

تاریخ دریافت: ۲۴ شهریور ۱۴۰۴ **تاریخ پذیرش:** ۳۰ مهر ماه ۱۴۰۴

چکیده

سرطان پستان سه‌گانه منفی (TNBC) فاقد گیرنده‌های قابل هدف درمانی است و شیمی‌درمانی متداول، علی‌رغم سمیت بالا و مقاومت اکتسابی، تنها گزینه استاندارد درمانی محسوب می‌شود. محورهای سیگنالینگ NF-κB و STAT3 در TNBC به‌طور مداوم فعال هستند و به‌عنوان محرک‌های انکوژنیک متقابل شناخته می‌شوند. ازاین‌رو، مهار همزمان آن‌ها یک راهبرد درمانی جذاب محسوب می‌گردد. بتا-سیتوسترول، فیتوسترول غالب دانه‌های *Allium cepa*، خواص ضدتکثیری گسترده‌ای نشان می‌دهد؛ با این حال، توانایی آن در تعامل همزمان با NFKB1 و STAT3 به‌صورت سیستماتیک بررسی نشده است. پروفایل‌سازی GC–MS روغن دانه *A. cepa*، بتا-سیتوسترول را به‌عنوان ترکیب اصلی با سهم ۸۰٪ شناسایی کرده است. آنالیز محاسباتی ADMET، اعتبارسنجی ایمونوسیتوشیمیایی اهداف از پایگاه داده Human Protein Atlas، و داکینگ مولکولی با AutoDock Vina علیه NFKB1 (PDB: 5AX3) و STAT3 (PDB: 7LET) انجام گرفت. فعالیت ضدسرطانی در سلول‌های MDA-MB-231 از طریق سنجش MTT ارزیابی شد و مکانیسم آپوپتوز با فلوسیتومتری Annexin V-FITC/PI مشخص گردید. بتا-سیتوسترول دارای پروفایل دارویی مطلوب، توزیع پیش‌بینی‌شده در میتوکندری، و فقدان جهش‌زایی ژنوتوکسیک گزارش شد. داکینگ انرژی‌های اتصال 7.0- و 6.7- کیلوکالری بر مول را به‌ترتیب برای STAT3 و NFKB1 نشان داد که عمدتاً از طریق برهمکنش‌های هیدروفوبیک ایجاد می‌شوند. سنجش MTT سمیت سلولی وابسته به غلظت را آشکار کرد (IC_{50} = 39.56 µM؛ 72h؛ F = 113.8، $p < 0.0001$). فلوسیتومتری القای معنادار آپوپتوز اولیه (30.7 ± 2.5%) و آپوپتوز دیررس (20.3 ± 4.4%) را در مقایسه با سطوح پایه ناچیز در گروه کنترل تأیید کرد. بتا-سیتوسترول همراه با قدرت اتصال محاسباتی دوگانه به NFKB1 و STAT3، فعالیت آپوپتوزی قوی در سلول‌های TNBC از خود نشان می‌دهد و بدین‌ترتیب پایه مکانیستی برای توسعه ترجمانی بیشتر آن به‌عنوان داوطلب درمانی دو محوره در سرطان پستان سه‌گانه منفی فراهم می‌آورد.

کلید واژه ها

بتا-سیتوسترول؛ سرطان پستان سه‌گانه منفی؛ NFKB1؛ STAT3؛ آپوپتوز؛ MDA-MB-231.

DOI: 10.30473/ijac.2026.77606.1345